ARTICLE

Bridging Interactions and Selective Nanoparticle Aggregation Mediated by Monovalent Cations

Dawei Wang,[†,‡] Baudilio Tejerina,[§] István Lagzi,[‡] Bartlomiej Kowalczyk,[‡] and Bartosz A. Grzybowski[‡,§,⊥,*]

[†]School of Materials Science and Engineering, Northwestern Polytechnical University, Xi'an 710072 P. R. China and [‡]Department of Chemical and Biological Engineering, [§]Non-equilibrium Energy Research Center (NERC), and [⊥]Department of Chemistry, Northwestern University, 2145 Sheridan Road, Evanston, Illinois 60208, United States

ABSTRACT Selective aggregation and precipitation of like-charged nanoparticles (NPs) covered with carboxylate ligands can be induced by different monovalent cations. The ordering of critical concentrations required for NP precipitation is $Cs^+ \gg K^+ > Li^+ > Na^+ > Rb^+$ and does not correlate with the size of hydrated cations M^+, nor can it be predicted by the Hofmeister series. On the other hand, different anions have no effect on the precipitation trends. These observations are rationalized by a theoretical model combining the elements of the DLVO theory with molecular-level calculations. The key component of the model is the cation-specific binding of various metal cations to the carboxylate ligands.

KEYWORDS: nanoparticles · bridging interaction · precipitation · selective aggregation · modeling

Nanoparticle (NP) aggregation induced by metal cations, M^+, has been used as a route to nanostructured materials,[1] and as a basis for detection schemes[2,3] in which NP−M^+−NP "bridging" changes the electrodynamic coupling between particles' cores[4] and translates into the solution's color change. In most of these applications, multivalent ions were used[5] to bridge charged ligands (typically, carboxylate-terminated molecules[5,6]) strongly, though with little selectivity (*e.g.*, NPs covered with carboxylate groups can be aggregated/precipitated by a range of divalent cations, including Ba^{2+},[7] Pd^{2+},[2,7] Cd^{2+},[2,7] Hg^{2+},[2,7] Cu^{2+},[8,9] Fe^{2+},[9] or Zn^{2+}[7,8,10]). In contrast, monovalent ions are thought to bind to functionalized ligands relatively weakly, and are therefore treated as electrolytes. If these electrolytes cause NP aggregation, this phenomenon is usually explained as resulting from the screening of electrostatic repulsions between the particles. Any dependence of critical salt concentration (CSC) necessary for NP aggregation on the nature of the salt is then attributed to the size of hydrated ions[11] or to the abilities of ions to change the structure of water (the so-called specific-ion effects, including the Hofmeister series ranking).[12,13] Here, we combine experiments with theory to show that these existing descriptions are incomplete and that different monovalent cations have different propensities for bridging interactions and for concomitant NP aggregation. Specially, we study systematically the aggregation of AuNPs coated with 11-mercaptoundecanoic acid ($HS(CH_2)_{10}COOH$, MUA) in the presence of different alkali halides (MCl, M = Li^+, Na^+, K^+, Rb^+ and Cs^+), as well as other salts of monovalent cations. We show that the order of salt concentrations required for AuNPs' aggregation is CsCl ≫ KCl > LiCl > NaCl > RbCl. It does not correlate with the size of hydrated cations M^+, nor can it be predicted by the Hofmeister series. At the same time, we show that the aggregation trends do not noticeably depend on the nature of anions. To rationalize these results, we implement molecular-level calculations that account for the hydration/dehydration of metal ions and for specific binding interactions between metal ions and charged groups on NP surfaces. When these ion-specific effects are combined with van der Waals (vdW) and electrostatic interactions (as in the DLVO theory[14]) between the NPs, they can explain the experimental precipitation trends. Our observations suggest that monovalent cations can be used as selective agents for NP aggregation and assembly and can therefore have ramifications for NP separations or synthesis of "hierarchical" nanostructured materials.[15,16]

RESULTS

Our experiments were based on AuNPs with the diameters of metal cores of either 6.5 ± 0.8 or 4.5 ± 0.6 nm (Figure 1a) and prepared according to a procedure[17] de-

*Address correspondence to grzybor@northwestern.edu.

Received for review September 24, 2010 and accepted November 16, 2010.

Published online December 23, 2010. 10.1021/nn1025252

scribed in detail in the Methods section. These AuNPs were coated with self-assembled monolayers, SAMs,[18,19] of 11-mercaptoundecanoic acid, MUA (pK_a = 6−8 for a MUA SAM on a curved surface[20,21]). To fully deprotonate the carboxylic groups of the MUA ligands, the pH of the AuNP solution was adjusted to ~11.5 by the addition of tetramethylammonium hydroxide, $N(CH_3)_4OH$). Aqueous solutions of alkali halides (MCl, 0.5−2 M, with pH ≈ 11.5 adjusted with $N(CH_3)_4OH$), as well as other salts ($NaNO_3$, Na_2SO_4), were used to titrate the AuNPs.

In a typical experiment, a stirred solution of AuNPs (2 mM, in terms of gold atoms) was titrated with small aliquots (20 μL) of a given salt solution. After each addition, the mixture was allowed to equilibrate until the UV−vis spectra of the solutions stabilized (typically, within a few hours, but some salts required up to 1−2 days, see ref 22), and the AuNP solution was then characterized by dynamic light scattering (DLS) for the size distribution and by the UV−vis for the concentration of the NPs in solution, c_{NP} (estimated from the intensity of the surface plasmon resonance, SPR, band centered at ~520 nm[23]). In terms of the graphical presentation of the results, we note that (i) if precipitation did not occur, the c_{NP} *vs* c_{salt} were straight lines reflecting dilution of the sample; (ii) if, however, precipitation took place, the curves featured a drop around some critical amount of added salt (Figure 1b). Finally, unless otherwise stated, all experiments were performed at ~25 °C.

We begin by noting that for a given cation, the nature of the anions has no noticeable effect on the NP aggregation behavior. This is illustrated in Figure 2a, where the AuMUA NPs were titrated with NaCl, $NaNO_3$, or Na_2SO_4. Although the anions in these salts have different valence and/or size, the titration curves are similar to one another and the NPs precipitate at CSC ≈ 30 mM.

In contrast, the nature of the M^+ cations does matter for the bridging and precipitation behavior. This is illustrated in Figure 2b which shows titration curves for five alkali chlorides. As seen, the cations have markedly different effects on the NPs' stability in solution. For Na^+, K^+, Li^+, Rb^+, the aggregation CSC thresholds follow the $Rb^+ < Na^+ < Li^+ < K^+$ order. No precipitation, however, is observed for Cs^+ even at salt concentration as high as 0.15 M, Also, as evidenced by DLS, for Na^+, K^+, Li^+, Rb^+, the addition of salt causes gradual aggregation of the NPs with precipitation occurring when the aggregates reach micrometer dimensions. Before precipitation takes place, the sizes, *d*, of the aggregates follow the trend "inverse" to that of the CSC —that is, for a given salt concentration, below CSC, $d_{Cs^+} < d_{K^+} < d_{Li^+} < d_{Na^+} < d_{Rb^+}$ (Figure 2c).

We make three further comments regarding these results. First, the general CSC trend $Rb^+ < Na^+ < Li^+ < K^+ \ll Cs^+$ is preserved for NPs of different sizes, although the specific CSC values change. In particular,

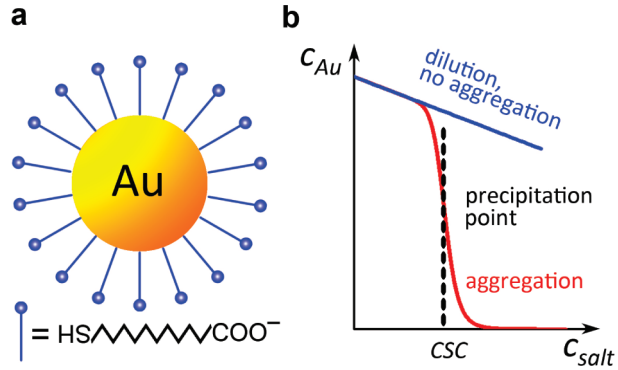

Figure 1. (a) Scheme of an AuMUA NP. (b) Graphical illustration of the stability of AuNPs during titration with a salt solution. The precipitation point is thermodynamically defined as the inflection point of the titration curve (the red curve), at which the chemical potentials of the free-NP and the aggregated-NP phases are equal. The salt concentration at the precipitation point is defined as the critical salt concentration (CSC).

when NPs become smaller, CSC increases (Figure 2d), which can be attributed to the fact that with these smaller NPs the area of contact and the number of $-COO^-M^+-\ ^-OOC-$ "bridges" decrease so that achieving precipitation requires higher salt concentrations. Second, we note that the precipitation trends cannot be explained by (correlated with) the size of the hydrated cations (the expected ordering of CSC would be $Li^+ > Na^+ > K^+ \approx Rb^+ \approx Cs^+$, based on the theory proposed in ref 11 and hydrated radii of Li^+ = 0.38 nm, Na^+ = 0.36 nm, K^+ = 0.33 nm, Rb^+ = 0.33 nm, and

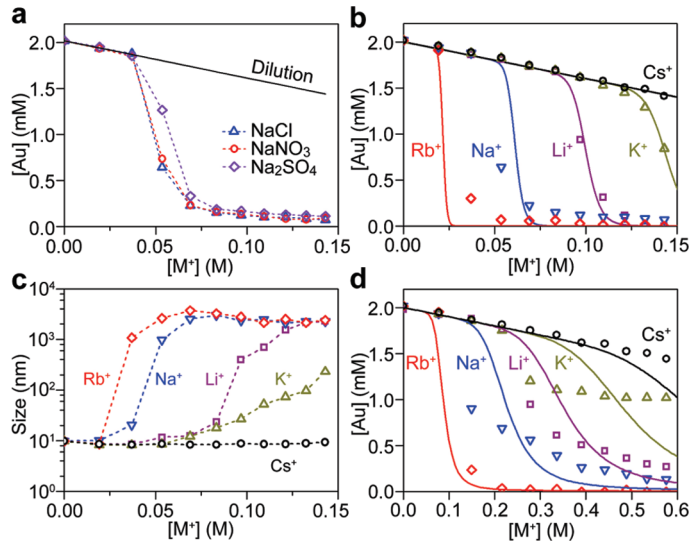

Figure 2. (a) Concentration of free AuNPs in solution as a function of the concentration of salts having different anions. (b) Solution concentration of free, 6.5 nm AuNPs as a function of the concentration of various salts MCl added. Markers correspond to experimental data, solid lines are the modeled precipitation trends. (c) The average hydrodynamic diameters (determined by DLS) of aggregates of 6.5 nm AuNPs plotted as a function of the concentration of added salts, MCl. Dashed lines are used to guide the eye (*i.e.*, they are not calculated). (d) Solution concentration of free, 4.5 nm AuNPs as a function of the concentration of various salts MCl added. Markers correspond to experimental data, solid lines are the modeled precipitation trends. In all graphs, the markers represent averages of a minimum of eight independent measurements for each condition, error bars are not included since they are on the order of the marker size.

Cs^+ = 0.33 nm, taken from ref 24), or by the typical Hofmeister series[13] $Li^+ < Na^+ < K^+ < Rb^+ < Cs^+$. Third, the aggregated NPs can be redissolved by the addition of water. This "reversibility" indicates that, at all salt concentrations, the system is equilibrated and the free-NP and aggregated-NP phases have the same chemical potentials.

THEORETICAL ANALYSIS

To rationalize the precipitation trends, we have developed a model that accounts for the vdW and electrostatic interactions between AuNPs and also for the "cation-specific" bridging of the carboxylate groups. At equilibrium, the relationship between concentration of free NPs in solution, c_f, and that of aggregated NPs, c_a, is determined by the equality of chemical potentials between these two phases.[25] It thus follows that $c_f = c_a \exp(\Delta u°/(k_B T))$, where $\Delta u°$ is the change in free energy associated with NP aggregation. Typically, the dominant contributions to $\Delta u°$ come from the van der Waals and electrostatic energies of interaction between the NPs. In our system, however, the dependence of titration curves on the nature of metal cations suggests that the specific ion effects, that is, the bridging interaction between M^+ and deprotonated MUA, should also be taken into account. Using a previously described model[25] of pairwise interactions between NPs, $\Delta u°$ can be approximated as $\Delta u° = n u_{total}/2$, where $n \approx 6$ is the average number of nearest neighbors in orderless NP aggregates, $u_{total} = u_{vdW} + u_{ES} + u_B$ is the total energy for two NPs at contact, and u_{vdW}, u_{ES}, and u_B are, respectively, the vdW, the electrostatic, and the bridging interaction energies. While u_{vdW} can be calculated on the basis of classical/continuum theories alone, the calculation of u_{ES} and u_B involves terms that describe cation-specific M^+−NP interactions and needs to be treated by quantum-mechanical methods. We emphasize that even though the model we are about to present yields realistic results, it requires simplifying (yet, we believe, physically reasonable) assumptions.

vdW Interactions. The vdW interactions, u_{vdW}, between two NPs can be approximated as

$$u_{vdw} = -\frac{A}{3}\left[\frac{R_c^2}{d^2 - 4R_c^2} + \frac{R_c^2}{d^2} + \frac{1}{2}\ln\left(1 - \frac{4R_c^2}{d^2}\right)\right]$$

where $A = 4 \times 10^{-19}$ J is the Hamaker constant for gold across water,[24] R_c is the radius of the NPs' metal cores (R_c = 3.25 or 2.25 nm in our experiments), and $d = 2(R_c + \delta) + L$ is the distance between NPs' centers, where $\delta \approx 1.63$ nm[17] is the thickness of the MUA SAM on AuNPs, and L is the "length" of the salt bridge and approximated as twice the length of the $-COO^- - M^+$ bonds, r_{COOM} (this parameter is calculated by quantum mechanical methods as described below).

Electrostatic Interactions. Electrostatic interactions, u_{ES}, between charged NPs in ionic solution are derived from the appropriate electrostatic potentials, φ, *via* thermodynamic integration[26,27] and account for "charge regulation" at the NPs' surface.[28] Briefly, the electrostatic potential around the NPs, φ, is well approximated by the linearized Poisson−Boltzmann equation, $\nabla^2\varphi = \kappa^2\varphi$, where $\kappa^{-1} = (\varepsilon\varepsilon_0 k_B T/(2N_A c_{M^+} e^2))^{1/2}$ is the Debye screening length, ε is the relative permittivity of the solvent ($\varepsilon \approx 80$ for water), ε_0 is the vacuum permittivity, k_B is the Boltzmann's constant, T stands for temperature, N_A is the Avogadro constant, c_{M^+} is the concentration of metal cations M^+ (here, Li^+, Na^+, K^+, Rb^+ or $Cs^{\cdot+}$), and e denotes elementary charge. The equilibrium between metal cations adsorbed onto the negatively charged NP surface and those free in solution is determined by

$$\frac{N_{A^-} x_{M^+}}{N_{AM}} = \exp\left(-\frac{\Delta G_d - e\varphi_s}{k_B T}\right)$$

where N_{A^-} and N_{AM} are the numbers of, respectively, counterion-free, deprotonated MUA ligands and counterion-bound, deprotonated MUA ligands, x_{M^+} is the molar fraction of cation M^+ in solution, φ_s is the electrostatic potential at the NP surface, and ΔG_d (calculated in the next section) is the free energy of desorption/dissociation of M^+ from the negatively charged NP surface.[28] Thus, the surface charge density, can be expressed as

$$\sigma = -\frac{e\Gamma}{1 + x_{M^+}\exp\left(\frac{\Delta G_d - e\varphi_s}{k_B T}\right)}$$

where Γ is the surface density of all ligands (both protonated and deprotonated; $\Gamma \approx 4.7$ nm^{-2} for SAM on AuNP[29]). Since the relative permittivity of a SAM ($\varepsilon_{SAM} \approx 2$, ref 25) is small compared to that of water (the solvent in our experiments), the surface charge density may also be written as $\sigma = -\varepsilon\varepsilon_0 \nabla\varphi_s \cdot \vec{n}$, where $\vec{n}$ is the outward surface normal. The boundary conditions at the surfaces of interacting NPs are linearized about the potential of an isolated particle, φ_∞, such that $-\varepsilon\varepsilon_0 \nabla\varphi_s \cdot \vec{n} = S - C\varphi_\infty$, where $S = \sigma(\varphi_\infty) - (\partial\sigma/\partial\varphi)_\infty \varphi_\infty$ and $C = -(\partial\sigma/\partial\varphi)_\infty$. After some algebra, the electrostatic interaction energy between two like-charged NPs can be derived as

$$u_{es} = \pi\varepsilon\varepsilon_0 R\left[\frac{\varphi_s^2}{\Delta}\ln(1 - \Delta^2) + \frac{2\varphi_s^2}{|\Delta|}\arctan(|\Delta|)\right]$$

where the coefficient $\Delta = (C - \varepsilon\varepsilon_0\kappa)/(C + \varepsilon\varepsilon_0\kappa)$ depends on $C = -\partial\sigma/\partial\varphi|_{\varphi=\varphi_\infty}$,[25] which is the derivative of the surface charge with respect to the potential of an isolated NP, φ_∞.

The Dissociation Energy ΔG_d. One of the key parameters in the calculation of electrostatic interactions (*cf.* above), is the free energy of dissociation of M^+ cations from the deprotonated COO^- groups on the particle. Since entropic gain due to dissociation is approximately constant for different cations,[30] we focus on the enthal-

TABLE 1. Data Obtained from DFT Calculations

	Li^+	Na^+	K^+	Rb^+	Cs^+
r_{COOM} (Å)	1.98	2.51	2.83	3.02	3.18
ΔG_d (10^{-20} J)[a]	0.33	0.58	0.16	1.09	0.00

[a]The values shown here are relative to that of Cs^+, $\sim 2.72 \times 10^{-20}$ J.

pic component. Our quantum mechanical calculations are based on a model describing the dissociation of alkali metals from acetates (mimicking the head groups of MUA), $CH_3COO^- \cdot M^+(aq) \rightarrow CH_3COO^-(aq) + M^+(aq)$; while simplified, this model takes into account the solvent (water) explicitly.

We used the density functional theory (DFT) method,[31,32] with the hybrid functional B3LYP.[33−36] The standard 6-31G(*d,p*) basis set (ref 37 for H, ref 38 for Li, ref 39 for C, N, O, and Na, ref 40 for K) augmented with a set of *d*-polarization functions on C, N, O, Li, Na, and K was used (ref 41 for C, N, O and Li, ref 42 for Na, ref 43 for K). To improve the description of the electron density of the lone-pairs on the water molecules and the anionic nature of the carboxylate groups, a set of diffuse functions was added to the oxygen atoms.[44] Electron density of the heavier alkaline metals, Rb and Cs, was described using effective core potentials with the corresponding basis functions.[45] The basis functions were obtained from the Basis Set Exchange Software and the Environmental Molecular Science Laboratory basis set library at the Pacific Northwest National Laboratory,[46,47] through its online portal. The solvation effects were taken into account by explicitly including the molecules of water. The hydrates were simulated by gradual and systematic addition of water molecules to the metal−acetate complex and optimizing the resulting structures. Up to 24 water molecules were considered per metal cation; of these, the structure with the lowest energy was chosen. All the calculations were carried out using the GAMESS[48] program with a graphical user interface, QC-Lab.[49] The stationary structures were characterized as minima on their respective potential energy surfaces by computing the Hessian of energy (second derivatives of energy with respect to the nuclear coordinates) and analyzing the vibration normal modes of the system. The Hessians were calculated numerically using double nuclear displacements. The zero-point energy corrections were calculated using the harmonic approximation.

Once the structure of carboxylate/metal/water complexes were determined, the dissociation energies ΔG_d were calculated as the difference between the energies of the hydrated complexes and of the energies of the hydrated but separated components.

Bridging Interactions. Compared with the ES repulsions, the vdW attractions between small NPs are weak and insufficient to cause their aggregation/precipitation.[25,50,51] On the other hand, the aggregation/precipitation of like-charged NPs can be induced by the bridging ions.[52] Here, the bridging energy, u_B, is taken as linearly proportional to the negative desorption energy ΔG_d, that is, $u_B = -f\Delta G_d$, where f is a proportionality constant. This approximation accounts—in the simplest possible way—for the fact that the bridging between SAMs is not necessarily a simple "sum" of the individual metal-acetate bindings, and the geom-

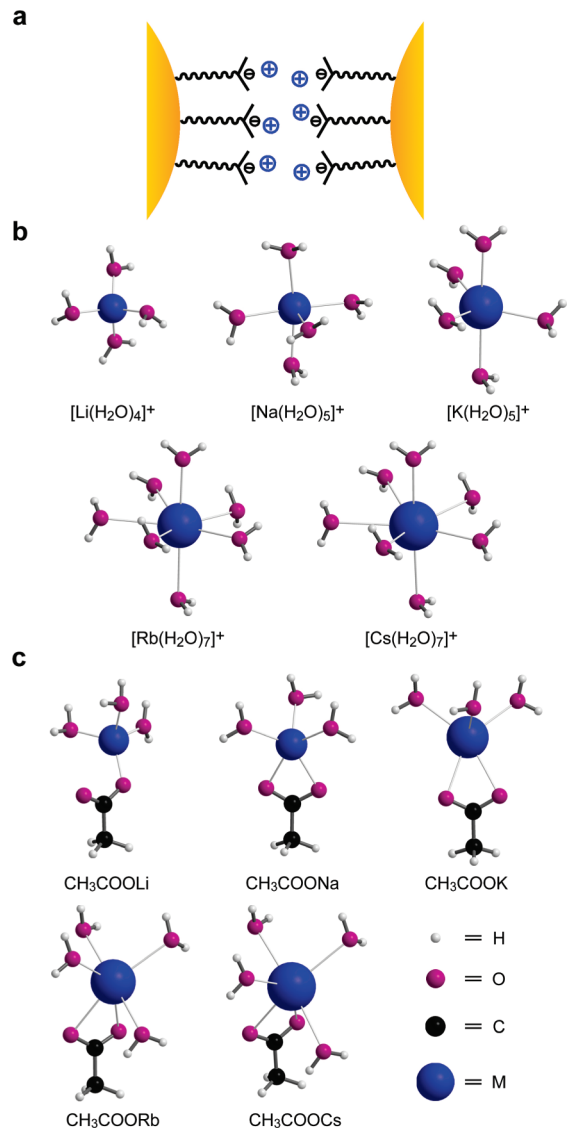

Figure 3. (a) Schematic representation (not drawn to scale) of the bridging interactions between metal cations (blue circles) and the carboxylate groups on two interacting NPs. (b) Minimum energy structures of the hydrated metal cations M^+/nH_2O. The hydration index of the metal cations was determined by topological analysis of the electrons density.[56] The hydration indices increase with the atomic number so that four molecules of water coordinate to Li^+, five to Na^+ and K^+, and seven to Rb^+ and Cs^+. (c) Minimum energy structures of the $CH_3COO\text{-}M^+/nH_2O$ clusters obtained from DFT simulations. The position of the Li^+ cation is characterized by the monodentate acetate−metal binding. In the heavier metals, however, the acetate group forms bidentate complexes in which both oxygen atoms of the carboxylic group coordinate to the metal. The number of water molecules coordinated to the metallic ion is related to the ion's size: three for the acetates of Li^+, Na^+ and K^+ and four molecules for Rb^+ and Cs^+.

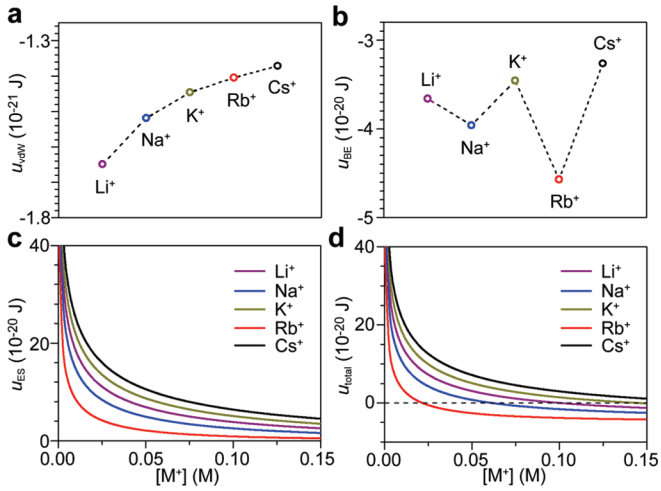

Figure 4. Energies of (a) vdW interactions (u_{vdW}), (b) bridging interactions (u_B), (c) ES interactions (u_{ES}), and (d) total interaction ($u_{total} = u_{vdW} + u_B + u_{ES}$) calculated for 6.5 nm AuNPs using the model described in the text. The horizontal, dashed line indicates $u_{total} = 0$.

etry of the bridge is likely not a simple superposition of the geometries of independent metal−acetate complexes; in this spirit, the parameter *f* is heuristic and should be construed as a free parameter of the model.

DISCUSSION

The calculated lengths of the $-COO^- - M^+$ bonds, r_{COOM}, and the desorption energies, ΔG_d, are listed in Table 1 and the minimum-energy structures of the hydrated cations $M^+(H_2O)_n$, and of the carboxylate/metal/water complexes obtained from DFT calculations are shown in Figure 3 panels b and c, respectively. To reproduce the experimental precipitation trends, the vdW, electrostatic, bridging, and the total interaction energies were calculated (see Figure 4a−d) with *f* being the only fitting parameter. The best-fit value of *f* (*f* = 1.2 for 6.5 nm NPs and *f* = 0.2 for 4.5 nm NPs) was determined against experimental titration curves with the condition for precipitation point $\Delta u^\circ = u_{total} = 0$ (*cf.* Figure 1b and 4d). The theoretical titration curves are included in Figure 2b,d as solid lines. Overall, the results of the simulations agree well with experimental observations and lead to the following conclusions:

(1) The role of vdW attractions. Compared with electrostatic and/or bridging interactions, the vdW interactions between NPs (coated with relatively long ligands used here) are weak (~10^{-21} J) and unable to induce the NP aggregation/precipitation alone. In addition, since the magnitude of these interactions increases with decreasing r_{COOM} (so that the NPs can get closer together), one would expect that these interactions cause precipitation in the order $Li^+ < Na^+ < K^+ < Rb^+ < Cs^+$ (related with bond length of COOM), that is, an order not observed in experiments (see Figure 4a).

(2) The role of bridging attractions. It should be noted that a model accounting only for the electrostatic and the vdW interactions predict the precipitation to be much less abrupt than seen in experiments and also not complete (specifically, less than 50% of the NPs are expected to be precipitated). The bridging attractions (on the order of 10^{-20} J) between the cations and carboxylate groups are stronger than the vdW attractions and comparable with the electrostatic interactions at high salt concentration—they are therefore essential for the NP precipitation.

(3) The experimental ordering of CSCs and the "sharpness" of precipitation curves are due to the nonmonotonic ordering of ΔG_d and, consequently, of the bridging interactions (Figure 4b). These energies follow neither the order of the hydrated cations' size, nor the Hofmeister series (as described above). The ion-specific desorption energies determine the ordering of electrostatic energies and of bridging energies, and subsequently account for the specific precipitation sequence (Figure 4d).

(4) Since the effective area of contact scales with particle size as $A_{eff} = 2\pi R\lambda$[28,50] (where *R* is NP radius and λ is characteristic length scale of molecular dimensions over which the MUA ligands can stretch or compress when forming salt bridges), the bridging energies are stronger for larger (here, 6.5 nm) than for smaller (4.5 nm) NPs. This dependence might explain why for all cations, the CSCs are smaller for larger NPs (*i.e.,* it takes less cations to cause precipitation of larger particles).

CONCLUSIONS

We described and explained the precipitation of like-charged NPs induced by monovalent metal cations. This phenomenon illustrates the importance of the ion-specific hydration and salt bridging effects. The selective aggregation/precipitation of NPs could be used for the controlled self-assembly of NPs into specific ordered materials. This system could also be extended to other NPs with different types of metal cores or coated with different ligands, to prepare multifunctional materials. Our work may also provide molecular-level insights into the specific ion effects in colloidal chemistry, polymer science, and biological systems.[53−55]

METHODS

Nanoparticle Synthesis and Functionalization. ***Stock Solution of Seed AuDDA NPs with the Diameters of Metal Cores ≈ 2−4 nm.*** A 370.2 mg portion of dodecylamine (DDA) and 461.8 mg of didodecyldimethylammonium bromide (DDAB) were dissolved in 11 mL of toluene, followed by the addition of 39.4 mg of $HAuCl_4 \cdot 3H_2O$ under sonication (~10 min). A fresh solution of tetrabutylammonium borohydride (TBAB) and DDAB was prepared by dissolving 97.6 mg of TBAB and 184.8 mg of DDAB in 4.8 mL of toluene under sonication and was injected to the vigorously stirred $HAuCl_4 \cdot 3H_2O$ solution. The thus prepared solution of seed Au-DDA nanoparticles was stirred for ~24 h at room temperature.

Growth Solution. A 6.298 g portion of DDA and 2.514 g of DDAB were dissolved in 136.1 mL of toluene, followed by the addition of 535.3 mg of $HAuCl_4 \cdot 3H_2O$ under sonication (~10 min).

Synthesis of AuDDA NPs with the Diameters of Metal Cores of 4.5 and 6.5 nm. To prepare 4.5 nm AuDDA NPs, 5.5 mL of seed solution was added to 35.3 mL of the growth solution. A fresh solution of anhydrous hydrazine (N_2H_4) and DDAB was prepared by dissolving 89.9 mg of N_2H_4 and 0.649 g of DDAB in 13.6 mL of toluene, and then added dropwise over ~30 min to the vigorously stirred NP solution. Thus prepared solution was stirred for ~24 h at room temperature.

The size of AuDDA NPs was controlled by adjusting the ratio of seed solution to the growth solution (in terms of Au content, specifically: ~1:7 for 4.5 nm AuDDA NPs, and ~1:20 for 6.5 nm AuDDA NPs).

Synthesis of AuMUA NPs. A toluene solution of AuDDA NPs (30−50 mL, ~250 μmol) was quenched with 50 mL of methanol. The precipitate formed was allowed to settle down, and the supernatant was discarded. The precipitate was redissolved in 30 mL of toluene; 218.4 mg of 11-mercaptoundecanoic acid (MUA) was dissolved in 20 mL of CH_2Cl_2, and then added to the NP solution. The AuMUA NPs formed and precipitated from toluene and were allowed to settle down over ~2 h. The supernatant was discarded. The NP precipitate was washed with 3 × 50 mL of CH_2Cl_2 and then redissolved in 10 mL of methanol; 100 μL of tetramethylammonium hydroxide (TMAOH, 25 wt % solution in methanol) was added to the NP solution causing precipitation of the deprotonated AuMUA NPs. The supernatant was then again discarded. The deprotonated AuMUA NPs were washed with 3 × 50 mL of actone and methanol. Finally, the NPs were dried under air flow and then dissolved in ~10 mL of DI water. Thus prepared AuMUA NPs were filtered through a microfilter (pore size, ~0.2 μm). The yield was ~80%. The deprotonated AuMUA NPs were stable in solution for weeks.

Acknowledgment. This work was supported by the DARPA program (01-130130-00//W911NF-08-1-0143), the PEW scholars program (to B.A.G.) and the Nonequilibrium Energy Research Center which is an Energy Frontier Research Center funded by the U.S. Department of Energy, Office of Science, Office of Basic Energy Sciences under Award Number DE-SC0000989.

REFERENCES AND NOTES

1. Katz, E.; Willner, I. Integrated Nanoparticle−Biomolecule Hybrid Systems: Synthesis, Properties, and Applications. *Angew. Chem., Int. Ed.* **2004**, *43*, 6042–6108.
2. Kim, Y.; Johnson, R. C.; Hupp, J. T. Gold Nanoparticle-Based Sensing of "Spectroscopically Silent" Heavy Metal Ions. *Nano Lett.* **2001**, *1*, 165–167.
3. Liu, J.; Lu, Y. Accelerated Color Change of Gold Nanoparticles Assembled by DNAzymes for Simple and Fast Colorimetric Pb^{2+} Detection. *J. Am. Chem. Soc.* **2004**, *126*, 12298–12305.
4. Pinchuk, A. O.; Kalsin, A. M.; Kowalczyk, B.; Schatz, G. C.; Grzybowski, B. A. Modeling of Electrodynamic Interactions between Metal Nanoparticles Aggregated by Electrostatic Interactions into Closely-Packed Clusters. *J. Phys. Chem.* **2007**, *111*, 11816–11822.
5. Wuelfing, W. P.; Zamborini, F. P.; Templeton, A. C.; Wen, X.; Yoon, H.; Murray, R. W. Monolayer-Protected Clusters: Molecular Precursors to Metal Films. *Chem. Mater.* **2000**, *13*, 87–95.
6. Uchida, M.; Klem, M. T.; Allen, M.; Suci, P.; Flenniken, M.; Gillitzer, E.; Varpness, Z.; Liepold, L. O.; Young, M.; Douglas, T. Biological Containers: Protein Cages as Multifunctional Nanoplatforms. *Adv. Mater.* **2007**, *19*, 1025–1042.
7. Zhu, L.; Xue, D.; Wang, Z. Metallic Cation Induced One-Dimensional Assembly of Poly(acrylic acid)-1-dodecanethiol-Stabilized Gold Nanoparticles. *Langmuir* **2008**, *24*, 11385–11389.
8. Zamborini, F. P.; Hicks, J. F.; Murray, R. W. Quantized Double Layer Charging of Nanoparticle Films Assembled Using Carboxylate/(Cu^{2+} or Zn^{2+})/Carboxylate Bridges. *J. Am. Chem. Soc.* **2000**, *122*, 4514–4515.
9. Berchmans, S.; Thomas, P. J.; Rao, C. N. R. Novel Effects of Metal Ion Chelation on the Properties of Lipoic Acid-Capped Ag and An Nanoparticles. *J. Phys. Chem. B* **2002**, *106*, 4647–4651.
10. Aili, D.; Enander, K.; Rydberg, J.; Nesterenko, I.; Björefors, F.; Baltzer, L.; Liedberg, B. Folding Induced Assembly of Polypeptide Decorated Gold Nanoparticles. *J. Am. Chem. Soc.* **2008**, *130*, 5780–5788.
11. Laaksonen, T.; Ahonen, P.; Johans, C.; Kontturi, K. Stability and Electrostatics of Mercaptoundecanoic Acid-Capped Gold Nanoparticles with Varying Counterion Size. *ChemPhysChem* **2006**, *7*, 2143–2149.
12. Zhou, J.; Beattie, D. A.; Ralston, J.; Sedev, R. Colloid Stability of Thymine-Functionalized Gold Nanoparticles. *Langmuir* **2007**, *23*, 12096–12103.
13. Lopez-Leon, T.; Jodar-Reyes, A. B.; Bastos-Gonzalez, D.; Ortega-Vinuesa, J. L. Hofmeister Effects in the Stability and Electrophoretic Mobility of Polystyrene Latex Particles. *J. Phys. Chem. B* **2003**, *107*, 5696–5708.
14. Hunter, R. J. *Foundations of Colloid Science*, 2nd ed.; Oxford University Press Inc.: New York, 2001.
15. DeVries, G. A.; Brunnbauer, M.; Hu, Y.; Jackson, A. M.; Long, B.; Neltner, B. T.; Uzun, O.; Wunsch, B. H.; Stellacci, F. Divalent Metal Nanoparticles. *Science* **2007**, *315*, 358–361.
16. Glotzer, S. C.; Solomon, M. J. Anisotropy of Building Blocks and Their Assembly into Complex Structures. *Nat. Mater.* **2007**, *6*, 557–562.
17. Kalsin, A. M.; Fialkowski, M.; Paszewski, M.; Smoukov, S. K.; Bishop, K. J. M.; Grzybowski, B. A. Electrostatic Self-Assembly of Binary Nanoparticle Crystals with a Diamond-like Lattice. *Science* **2006**, *312*, 420–424.
18. Witt, D.; Klajn, R.; Barski, P.; Grzybowski, B. A. Applications, Properties and Synthesis of Omega-Functionalized *n*-Alkanethiols and Disulfides—The Building Blocks of Self-Assembled Monolayers. *Curr. Org. Chem.* **2004**, *8*, 1763–1797.
19. Love, J. C.; Estroff, L. A.; Kriebel, J. K.; Nuzzo, R. G.; Whitesides, G. M. Self-Assembled Monolayers of Thiolates on Metals as a Form of Nanotechnology. *Chem. Rev.* **2005**, *105*, 1103–1169.
20. Kalsin, A. M.; Kowalczyk, B.; Smoukov, S. K.; Klajn, R.; Grzybowski, B. A. Ionic-like Behavior of Oppositely Charged Nanoparticles. *J. Am. Chem. Soc.* **2006**, *128*, 15046–15047.
21. Leopold, M. C.; Black, J. A.; Bowden, E. F. Influence of Gold Topography on Carboxylic Acid Terminated Self-Assembled Monolayers. *Langmuir* **2002**, *18*, 978–980.
22. Upon the addition of the same amount of a salt solution, small AuNPs aggregated/precipitated more slowly than large AuNPs, especially for Li^+.
23. Kalsin, A. M.; Kowalczyk, B.; Wesson, P.; Paszewski, M.; Grzybowski, B. A. Studying the Thermodynamics of Surface Reactions on Nanoparticles by Electrostatic Titrations. *J. Am. Chem. Soc.* **2007**, *129*, 6664–6665.
24. Israelachvili, J. N. *Intermolecular and Surface Forces*, 2nd ed.; Academic Press: New York, 1991.
25. Bishop, K. J. M.; Kowalczyk, B.; Grzybowski, B. A. Precipitation of Oppositely Charged Nanoparticles by Dilution and/or Temperature Increase. *J. Phys. Chem. B* **2009**, *113*, 1413–1417.
26. Carnie, S. L.; Chan, D. Y. C.; Gunning, J. S. Electrical Double-Layer Interaction Between Dissimilar Spherical Colloidal Particles and Between a Sphere and a Plate—The Linearized Poisson−Boltzmann Theory. *Langmuir* **1994**, *10*, 2993–3009.
27. Verwey, E. J. W.; Overbeek, J. T. G. *Theory of the Stability of Lyophobic Colloids*; Elsevier: New York, 1948.
28. Bishop, K. J. M.; Wilmer, C. E.; Soh, S.; Grzybowski, B. A. Nanoscale Forces and Their Uses in Self-Assembly. *Small* **2009**, *5*, 1600–1630.
29. Leff, D. V.; Ohara, P. C.; Heath, J. R.; Gelbart, W. M. Thermodynamic Control of Gold Nanocrystal Size: Experiment and Theory. *J. Phys. Chem.* **1995**, *99*, 7036–7041.

30. Remko, M.; Fitz, D.; Rode, B. M. Effect of Metal Ions (Li^+, Na^+, K^+, Mg^{2+}, Ca^{2+}, Ni^{2+}, Cu^{2+}, and Zn^{2+}) and Water Coordination on the Structure and Properties of L-Arginine and Zwitterionic L-Arginine. *J. Phys. Chem. A* **2008**, *112*, 7652–7661.
31. Koch, W.; Holthausen, M. C. *A Chemist's Guide to Density Functional Theory*; 2nd ed.; Wiley-VCH, 2001.
32. Parr, R. G.; Yang, W. *Density Functional Theory*; Oxford University Press, 1989.
33. Stephens, P. J.; Devlin, F. J.; Chabalowski, C. F.; Frisch, M. J. Ab-initio Calculation of Vibrational Absorption and Circular Dichroism Spectra Using Density-Functional Force-Fields. *J. Phys. Chem.* **1994**, *98*, 11623–11627.
34. Hertwig, R. H.; Koch, W. On the Parameterization of the Local Correlation Functional. What Is Becke-3-LYP? *Chem. Phys. Lett.* **1997**, *268*, 345–351.
35. Lee, C.; Yang, W.; Parr, R. G. Development of the Colle−Salvetti Correlation-Energy Formula into a Functional of the Electron Density. *Phys. Rev. B* **1988**, *37*, 785–789.
36. Becke, A. D. Density−Functional Thermochemistry. 3. The Role of Exact Exchange. *J. Chem. Phys.* **1993**, *98*, 5648–5652.
37. Ditchfield, R.; Hehre, W. J.; Pople, J. A. Self-Consistent Molecular-Orbital Methods. 9. Extended Gaussian-Type Basis for Molecular-Orbital Studies of Organic Molecules. *J. Chem. Phys.* **1971**, *54*, 724–729.
38. Dill, J. D.; Pople, J. A. Self-Consistent Molecular Orbital Methods. 15. Extended Gaussian-Type Basis Sets for Lithium, Beryllium and Boron. *J. Chem. Phys.* **1975**, *62*, 2921–2923.
39. Hehre, W. J.; Ditchfield, R.; Pople, J. A. Self-Consistent Molecular Orbital Methods. 12. Further Extensions of Gaussian-Type Basis Sets for Use in Molecular Orbital Studies of Organic Molecules. *J. Chem. Phys.* **1972**, *56*, 2257–2262.
40. Rassolov, V. A.; Ratner, M. A.; Pople, J. A.; Redfern, P. C.; Curtiss, L. A. 6-31G* Basis Set for Third-Row Atoms. *J. Comput. Chem.* **2001**, *22*, 976–984.
41. Harihara, P. C.; Pople, J. A. Influence of Polarization Functions on Molecular-Orbital Hydrogeneration Energies. *Theor. Chim. Acta* **1973**, *28*, 213–222.
42. Francl, M. M.; Pietro, W. J.; Hehre, W. J.; Binkley, J. S.; Gordon, M. S.; DeFrees, D. J.; Pople, J. A. Self-Consistent Molecular-Orbital Methods. 23. A Polarization-Type Basis Set for 2nd Row Elements. *J. Chem. Phys.* **1982**, *77*, 3654–3665.
43. Rassolov, V. A.; Pople, J. A.; Ratner, M. A.; Windus, T. L. 6-31G* Basis Set for Atoms K Through Zn. *J. Chem. Phys.* **1998**, *109*, 1223–1229.
44. Spitznagel, G. W.; Clark, T.; Chandrasekhar, J.; Schleyer, P. v. R. Stabilization of Methyl Anions by First-Row Substituents. The Superiority of Diffuse Function-Augmented Basis Sets for Anion Calculations. *J. Comput. Chem.* **1983**, *3*, 363–371.
45. Leininger, T.; Nicklass, A.; Küchle, W.; Stoll, H.; Dolg, M.; Bergner, A. The Accuracy of the Pseudopotential Approximation: Nonfrozen-Core Effects for Spectroscopic Constants of Alkali Fluorides XF (X = K, Rb, Ca). *Chem. Phys. Lett.* **1996**, *255*, 274–280.
46. Feller, D. The Role of Databases in Support of Computational Chemistry Calculations. *J. Comput. Chem.* **1996**, *17*, 1571–1586.
47. Schuchardt, K. L.; Didier, B. T.; Elsethagen, T.; Sun, L.; Gurumoorthi, V.; Chase, J.; Li, J.; Windus, T. L. Basis Set Exchange: A Community Database for Computational Sciences. *J. Chem. Inf. Model.* **2007**, *47*, 1045–1052.
48. Schmidt, M. W.; Baldridge, K. K.; Boatz, J. A.; Elbert, S. T.; Gordon, M. S.; Jensen, J. H.; Koseki, S.; Matsunaga, N.; Nguyen, K. A.; Su, S.; *et al*. General Atomic and Molecular Electronic-Structure System. *J. Comput. Chem.* **1993**, *14*, 1347–1363.
49. Tejerina, B. QC-Lab, 2006. http://nanohub.org. DOI: 10254/nanohub-r1035.7.
50. Smoukov, S. K.; Bishop, K. J. M.; Kowalczyk, B.; Kalsin, A. M.; Grzybowski, B. A. Electrostatically "Patchy" Coatings *via* Cooperative Adsorption of Charged Nanoparticles. *J. Am. Chem. Soc.* **2007**, *129*, 15623–15630.
51. Bishop, K. J. M.; Grzybowski, B. A. "Nanoions": Fundamental Properties and Analytical Applications of Charged Nanoparticles. *ChemPhysChem* **2007**, *8*, 2171–2176.
52. Ojea-Jimenez, I.; Puntes, V. Instability of Cationic Gold Nanoparticle Bioconjugates: The Role of Citrate Ions. *J. Am. Chem. Soc.* **2009**, *131*, 13320–13327.
53. Zhang, Y.; Cremer, P. S. Interactions between Macromolecules and Ions: The Hofmeister Series. *Curr. Opin. Chem. Biol.* **2006**, *10*, 658–663.
54. Ninham, B. W.; Yaminsky, V. Ion Binding and Ion Specificity: The Hofmeister Effect and Onsager and Lifshitz Theories. *Langmuir* **1997**, *13*, 2097–2108.
55. Kunz, W.; Lo Nostro, P.; Ninham, B. W. The Present State of Affairs with Hofffieister Effects. *Curr. Opin. Colloid Interface Sci.* **2004**, *9*, 1–18.
56. Bader, R. F. W. *Atoms in Molecules: A Quantum Theory*; Oxford University Press: Oxford, 1990.